Dynamical characteristics of the vitrification process of an ideal system

1998 J. Phys.: Condens. Matter 10 11491

(http://iopscience.iop.org/0953-8984/10/49/035)

J. Phys.: Condens. Matter **10** (1998) 11491–11498. Printed in the UK PII: S0953-8984(98)96513-4

Dynamical characteristics of the vitrification process of an ideal system

T Odagaki, J Matsui and M Higuchi

Department of Physics, Kyushu University, Fukuoka 812-8581 Japan

Received 5 June 1998

Abstract. The dynamical characteristics of the vitrification process for a binary soft-sphere system are studied by means of an extensive molecular dynamics simulation. Using a Cole–Cole plot of the susceptibility, evidence is given for the first time of a fast process, which can be identified over a certain temperature range. Comparing with an ideal three-mode model in three dimensions, it is concluded that the fast process and the boson peak are related to the trapped motion.

1. Introduction

Liquids can be transformed into solids along two different paths; one is the crystallization path and the other is the vitrification path. In the vitrification process, a liquid solidifies keeping its structure. Thus one can regard the glass as a liquid which does not flow and is in a state under an extreme condition.

The dynamics of atoms during the vitrification process follows a completely different path to that for the crystallization process, which can be clearly seen in the temperature dependence of the generalized susceptibility. In fact, many experimental studies of the vitrification process have been carried out using neutron scattering [1, 2], light scattering [3] and dielectric measurements [4]. In most of these experiments, the imaginary part of the generalized susceptibility, $\chi''(\boldsymbol{q}, \omega)$, has been measured as a function of temperature. According to these experiments, in supercooled liquids, at least three different types of dynamics can be identified [1–5]:

(1) a slow relaxation, separated from the main peak, which moves to lower frequency as the temperature is reduced further [1–3];

(2) a so-called boson peak [2], whose position does not depend much on the temperature;

(3) a fast-relaxation process, which is observed over a limited temperature region [5].

In many systems, the relaxation time, τ_α, of the slow process can be fitted by the Vogel–Fulcher equation

$$\tau_\alpha \sim \exp[DT_0/(T - T_0)] \tag{1}$$

which diverges at a temperature T_0 known as the Vogel–Fulcher temperature. Here, T is the temperature and D, a positive constant, is called the fragility parameter. These characteristics of the dynamics have also been observed for a model glass former by computer simulation [6]. The assignment of these characteristics of the dynamics is the most important task in achieving an understanding of the glass-forming process.

0953-8984/98/4911491+08$19.50

In this paper, we study the dynamical characteristics of a binary soft-sphere model, in which particles interact with each other through a purely repulsive force. It is known [8] that the repulsive part of the molecular interaction plays the major role in the crystallization, in particular under high pressures. We believe that the present system is the simplest one that shows a glass transition, and that the properties observed in the glass-forming process for the soft-sphere system should be observed in the vitrification process in general. We report in section 2 the Cole–Cole plot [7] analysis of the generalized susceptibility for the binary soft-sphere system made to assign the dynamical modes. In section 3, we explain the ideal three-mode model in three dimensions [9]. From comparison of the results with simulation, we assert that (1) the slow process is related to the jump motion, (2) the fast process is due to the trapped diffusive motion and (3) the boson peak is due to localized oscillatory motions.

2. Cole–Cole analysis of the susceptibility

2.1. The model and procedure of simulation

We use a binary soft-sphere system [10]; the interparticle potential, $\phi_{\alpha\beta}(r)$, of two particles of the species α and β at a distance r is purely repulsive:

$$\phi_{\alpha\beta}(r) = \epsilon(\sigma_{\alpha\beta}/r)^{12} \qquad (\alpha, \beta = 1, 2) \tag{2}$$

where

$$\sigma_{\alpha\beta} = (\sigma_\alpha + \sigma_\beta)/2.$$

The total number of particles, N $(=N_1 + N_2)$, is 500, and the ratios of the atomic fractions, diameters and masses are $N_1/N_2 = 1$, $\sigma_1/\sigma_2 = 1.2$ and $m_1/m_2 = 2.0$, respectively. The temperature and the density of the system can be effectively reduced to one parameter known as the effective coupling constant [10]:

$$\Gamma_{\text{eff}} = (N/V)\sigma_{\text{eff}}^3(\varepsilon/k_B T)^{1/4} \tag{3}$$

where V is the volume, k_B is the Boltzmann constant and the effective diameter is defined by

$$\sigma_{\text{eff}}^3 = (\sigma_{11}^3 + \sigma_{12}^3 + \sigma_{21}^3 + \sigma_{22}^3)/4.$$

Note that Γ_{eff} is proportional to $T^{-1/4}$ when the density is fixed.

The simulation starts from the liquid state at $\Gamma_{\text{eff}} = 0.8$; we are using a constant-temperature simulation. The time step of the simulation is 0.001τ, where

$$\tau \equiv \sqrt{m\sigma_1^2/\epsilon}$$

is a microscopic timescale of the system. After the system is quenched to each measurement temperature and annealed, we switch to a microcanonical simulation and calculate the self-part of the generalized susceptibility

$$\chi_s(q, \omega) \equiv \chi_s'(q, \omega) + \mathrm{i}\chi_s''(q, \omega)$$

using the following equation [11]:

$$\chi_s(\boldsymbol{q}, \omega) = 1 + \frac{\mathrm{i}\omega}{T_{\text{total}}} \left\langle \sum_j \int_0^{T_{\text{total}}} \mathrm{d}t_0 \ \mathrm{e}^{\mathrm{i}\boldsymbol{q}\cdot\boldsymbol{r}_i(t_0)} \mathrm{e}^{-\mathrm{i}\omega t_0} \int_0^{t_0} \mathrm{d}t \ \mathrm{e}^{-\mathrm{i}\boldsymbol{q}\cdot\boldsymbol{r}_j(t)} \mathrm{e}^{\mathrm{i}\omega t} \right\rangle_i \tag{4}$$

where $\boldsymbol{r}_i(t)$ is the position of the ith atom at time t, which is computed directly by MD simulation. Here, T_{total} is the total number of time steps of the integration in equation (4),

which has to be sufficiently large. In our calculation, we have integrated up to 1 000 000 time steps, which corresponds to the order of ten nanoseconds. It has been shown that the freezing point and the glass transition point are at $\Gamma_{\rm eff} = 1.15$ and 1.58, respectively [10].

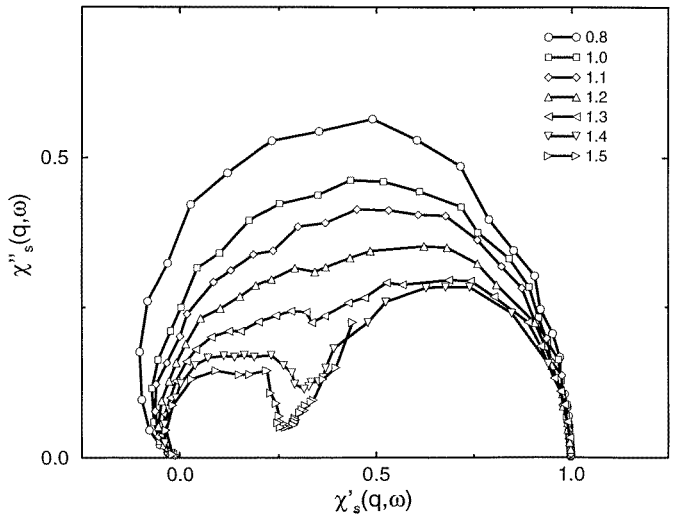

Figure 1. Cole–Cole plots of $\chi_s(q,\omega)$ at different temperatures. The numbers in the figure are values of the effective coupling constant, $\Gamma_{\rm eff}$, which is proportional to $T^{-1/4}$. The wavenumber $q = 2\pi/\sigma_1$ corresponds to the inverse interparticle distance. All of the data are averaged for two species. These curves are the result of one run of the MD simulation and the rapid variation of the curves is a good estimate of the error bars.

2.2. Results

The dynamical modes can be clearly seen in the Cole–Cole plot where the imaginary part of the susceptibility is plotted against the real part of the susceptibility for various values of the frequency. Figure 1 shows the Cole–Cole plot for our system obtained from the MD simulation. For the liquid state, $\Gamma_{\rm eff} = 0.8$, the plot is close to a semicircle except in the vicinity of the origin (where the frequency is very high). This indicates that the atomic motion in the liquid state is well described by a simple exponential relaxation, except at high frequencies where the high-frequency oscillation gives rise to the 'curled-over' behaviour of the plot. When the temperature is reduced, the shape of the semicircle becomes flattened and below the melting temperature, $\Gamma_{\rm eff} > 1.15$, the plot splits into two semicircles, separating out a slow dynamics.

The semicircle on the high-frequency side is considered to be mostly due to the oscillatory motion, since the high-frequency side of the semicircle goes to the negative side of the horizontal axis. Note that an arc appears at the right-hand shoulder of this semicircle. From a careful analysis we conclude that this arc is related to the fast process.

We determined the characteristic time of the fast process from the arc in the Cole–Cole plot. We plot the temperature dependence of the characteristic time in figure 2 as triangles, where the timescales of the slow process (the squares) and the microscopic process (the circles) obtained previously [6] are also shown. We conclude that the timescale of the fast process is independent of temperature in this region. We reported elsewhere [12]

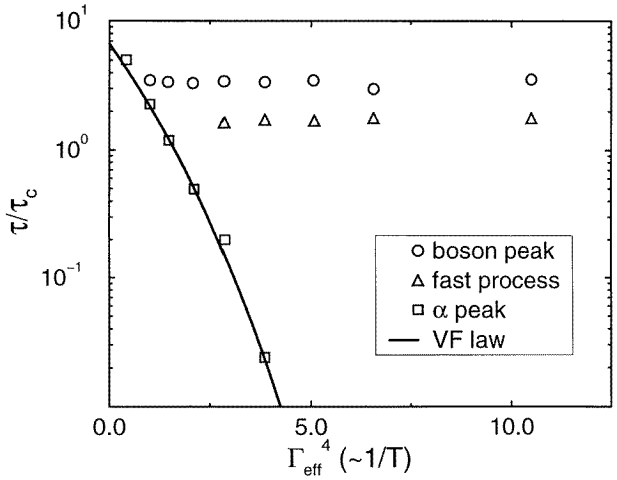

Figure 2. The temperature dependence of the characteristic time of the fast process (triangles). The squares and circles represent the characteristic time for the α-relaxation and the boson peak, respectively. The solid curve shows the Vogel–Fulcher law (1) with $D = 13.1$ and $T_0 = 11.8\epsilon/k_B$.

the wavenumber dependence of the susceptibility, and concluded that the fast process is produced on an atomic scale and that the slow process originates in the jump motion.

3. The ideal three-mode model

3.1. The model

In order to test the assignment of the modes described in section 2, we consider an ideal model in three dimensions consisting of three modes, an oscillatory motion, a trapped jump motion and a non-trapped jump motion. We consider an atom on a cubic lattice (the lattice constant is denoted by ℓ) which performs a harmonic oscillation around site $\boldsymbol{s}$ and denote the position of the atom by

$$\boldsymbol{x}(t) = \boldsymbol{s} + \boldsymbol{x}_0 \sin(\Omega t). \tag{5}$$

We assume that $\boldsymbol{s}$ follows two kinds of stochastic motion: one is the jump motion among the lattice sites, where the atom can make a jump only to adjacent sites with jump rate w; the other is the motion among decorated sites around a given lattice site. The distance and the rate of jumps between the lattice site and an additional site are denoted by a ($a < \ell$) and w_b ($w \leqslant w_b \leqslant \Omega$), respectively. Figure 3 shows these motions schematically.

According to a recent analysis of the wavenumber dependence of $\chi_s''(\boldsymbol{q}, \omega)$ for the soft-sphere system [13], the length scale $|\boldsymbol{x}_0|$ of the oscillatory motion is of the order of a few tens of per cent of the interparticle distance and that, a, for the stray motion is of the order of the interparticle distance. The frequency Ω is considered to be of the order of the Einstein frequency. Because of the random structure, most of the oscillatory modes are supposed to be localized and their frequency is distributed around the Einstein frequency.

We introduce the probability, $P(\boldsymbol{s}, t)$, that the atom is at site $\boldsymbol{s} \equiv \boldsymbol{n} + \boldsymbol{\sigma}$ at time t, when it started at site $\boldsymbol{s} = 0$ at time $t = 0$, where $\boldsymbol{n}$ is a lattice site and $\boldsymbol{\sigma}$ represents one of the decorated sites of $\boldsymbol{n}$. The conditional probability, $P(\boldsymbol{s}, t)$, is assumed to be determined by the master equations

$$\frac{\mathrm{d}}{\mathrm{d}t} P(\boldsymbol{n} + \boldsymbol{\sigma}, t) = w_b[P(\boldsymbol{n}, t) - P(\boldsymbol{n} + \boldsymbol{\sigma}, t)] \tag{6}$$

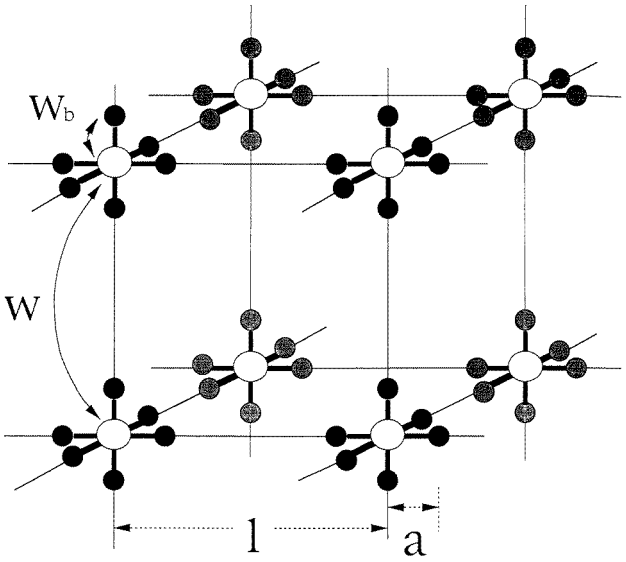

Figure 3. A schematic illustration of two kinds of stochastic jump motion in a three-dimensional lattice. The atom performs a long jump motion between the lattice sites, with jump rate w, and a short jump around each site, with jump rate w_b. It also independently performs an oscillatory motion, which is not shown.

and

$$\frac{\mathrm{d}}{\mathrm{d}t}P(\boldsymbol{n},t)=\sum_{\boldsymbol{n}'}wP(\boldsymbol{n}',t)+\sum_{\boldsymbol{\sigma}}w_bP(\boldsymbol{n}+\boldsymbol{\sigma},t)-6(w+w_b)P(\boldsymbol{n},t) \quad (7)$$

where the summation for $\boldsymbol{n}'$ is taken over the nearest neighbours of site $\boldsymbol{n}$ and the summation for $\boldsymbol{\sigma}\neq\boldsymbol{0}$ is taken over the decorating sites of $\boldsymbol{n}$. It is straightforward to show that, if $P(\boldsymbol{n},t)$ obeys equations (6) and (7), the Laplace–Fourier transform

$$\tilde{\tilde{P}}(\boldsymbol{q},u)\equiv\sum_{\boldsymbol{n}}\exp(\mathrm{i}\boldsymbol{q}\cdot\boldsymbol{n})\int_0^\infty P(\boldsymbol{n},t)\mathrm{e}^{-ut}\,\mathrm{d}t \quad (8)$$

is given by (see the appendix)

$$\tilde{\tilde{P}}(\boldsymbol{q},u)=\left\{u+6w+6w_b-\frac{6w_b^2}{u+w_b}-2w[\cos(q_x\ell)+\cos(q_y\ell)+\cos(q_z\ell)]\right\}^{-1}. \quad (9)$$

We obtain the generalized susceptibility from

$$\chi_s(\boldsymbol{q},\omega)=1+\mathrm{i}\omega\int_0^\infty F_s(\boldsymbol{q},t)\exp(\mathrm{i}\omega t)\,\mathrm{d}t \quad (10)$$

where the self-part of the intermediate scattering function, $F_s(\boldsymbol{q},t)$, is defined by

$$F_s(\boldsymbol{q},t)=\sum_{\boldsymbol{s}}\langle\exp\{\mathrm{i}\boldsymbol{q}\cdot[\boldsymbol{s}+\boldsymbol{x}_0\sin(\Omega t)]\}\rangle\,P(\boldsymbol{s},t). \quad (11)$$

Here $\langle\cdots\rangle$ denotes an average over the distribution of frequency Ω, which is introduced to take account of the inhomogeneity of the local configuration around the potential well. We employ the elliptic distribution as a simple example, where the density of states of Ω is given by

$$D(\Omega)=\begin{cases}\dfrac{2}{\pi\Delta}\left(1-\dfrac{(\Omega-\Omega_0)^2}{\Delta^2}\right)^{1/2} & \text{when } |\Omega-\Omega_0|\leqslant\Delta\\ 0 & \text{otherwise.}\end{cases} \quad (12)$$

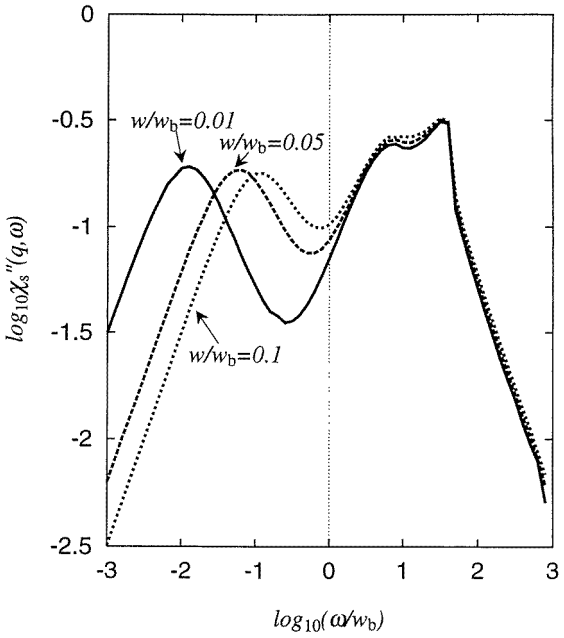

Figure 4. The imaginary part of the generalized susceptibility for the ideal three-mode model in three dimensions. We set $\boldsymbol{x}_0 = (0.15\ell, 0.15\ell, 0.15\ell)$, $a = 0.6\ell$, $\Omega_0 = 15w_b$, $\Delta = 9w_b$, $\boldsymbol{q} = (2/\ell, 2/\ell, 2/\ell)$ and $w/w_b = 0.01$ (solid curve), 0.05 (dashed curve) and 0.1 (dotted curve).

3.2. Generalized susceptibility and the Cole–Cole plot

In figure 4, we show the typical behaviour of the imaginary part of the generalized susceptibility, $\chi_s''(\boldsymbol{q}, \omega)$, for three different values of w.

We find that the position of the peak on the lower-frequency side, which is determined by non-trapped jumps, is given by w^{-1} and that the height of this peak does not change significantly even if w is varied. Note that it has been shown [14] that, when w obeys a power-law distribution, the relaxation time for this peak follows the Vogel–Fulcher law (1). Similarly, the position of the middle peak, which is determined by the trapped jump motion, is scaled by w_b and the height of this peak does not change significantly when w_b is varied.

The peak on the high-frequency side, which is determined by the oscillatory motion, appears at twice the frequency of the centre of the distribution, Ω_0. The height of this peak is scaled by the squared amplitude of the oscillatory motion, $|\boldsymbol{x}_0|^2$, i.e. the average potential energy of the oscillatory motion. This indicates that the peak can be scaled by the temperature, in agreement with results of reference [6]. We also confirmed that the peak height can be scaled by the square of the wavenumber.

Figure 5 shows a Cole–Cole plot of the generalized susceptibility. The peak determined by the non-trapped jump motion appears as a semicircle at the right-hand side, with the centre on the real axis, and the peak determined by the trapped jump motion appears as a central arc. The Cole–Cole plot shows a curl on the negative side of $\chi_s'(\boldsymbol{q}, w)$. Comparing figures 1 and 5, we can conclude that the slow process is produced by the non-trapped jump motion and that the fast process and the boson peak can be assigned to a trapped stochastic motion and to a localized oscillatory motion, respectively.

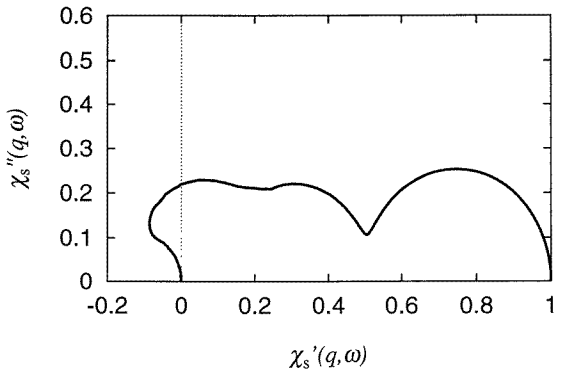

Figure 5. A Cole–Cole plot of the generalized susceptibility for the ideal three-mode model in three dimensions. We set $\boldsymbol{x}_0 = (0.1\ell, 0.1\ell, 0.1\ell)$, $a = 0.5\ell$, $w = 0.1w_b$, $\Omega_0 = 15w_b$, $\Delta = 9w_b$ and $\boldsymbol{q} = (2/\ell, 2/\ell, 2/\ell)$.

4. Discussion

In this paper we have discussed the gradual transition from the liquid to the solid state for the dynamical properties of a supercooled binary soft-sphere system obtained by MD simulation and presented evidence, for the first time, of the fast process in simulated supercooled liquids. In order to assign the dynamics observed in the simulation, we have introduced an ideal three-mode model in three dimensions. From the comparison of the behaviour of the Cole–Cole plot, we attribute the slowest mode to a concerted jump motion from a trapped site, the fast process to a trapped diffusion and the boson peak to a rapid oscillation in a trapped region. Since these modes are observed in the simple system with purely repulsive interaction, they must represent dynamical characteristics in any glass formers as observed in experiments [2–4], and other relaxation processes should be attributed to dynamics related to the degrees of freedom other than the translational motions of the centres of mass of the molecules. It should be noted that the dynamical singularities in the vitrification process can be understood in a unified manner by considering the divergence of various moments of the waiting time distribution for the non-trapped motion [15].

It should be remarked here that the intermediate scattering function, equation (11), of the ideal three-mode model shows an exponential decay with some modification due to the trapped motion [9]. This is simply due to the fact that the jump rate w for non-trapped motion is assumed to be a constant in this model. As we have shown elsewhere [15], the jump rate is likely to show a power-law distribution in glass formers, which leads to a stretched-exponential decay of the intermediate scattering function [16].

Acknowledgments

This work was supported in part by grants from the Ministry of Education, Science, Sport and Culture, the Sanyo Broadcasting Foundation and Corning Incorporated, Japan.

Appendix A. Derivation of equation (9)

First, we introduce the Laplace transform, $\tilde{P}(\boldsymbol{s}, u)$, of the conditional probability, $P(\boldsymbol{s}, t)$:

$$\tilde{P}(\boldsymbol{s}, u) = \int_0^\infty P(\boldsymbol{s}, t)\mathrm{e}^{-ut}\,\mathrm{d}t. \tag{A1}$$

The Laplace transforms of the master equations (6) and (7) read

$$u\tilde{P}(\boldsymbol{n}+\boldsymbol{\sigma}, u) - P(\boldsymbol{n}+\boldsymbol{\sigma}, t=0) = w_b[\tilde{P}(\boldsymbol{n}, u) - \tilde{P}(\boldsymbol{n}+\boldsymbol{\sigma}, u)] \tag{A2}$$

and

$$u\tilde{P}(\boldsymbol{n},u)-P(\boldsymbol{n},t=0)=\sum_{\boldsymbol{n}'}w\tilde{P}(\boldsymbol{n}',u)+\sum_{\boldsymbol{\sigma}}w_b\tilde{P}(\boldsymbol{n}+\boldsymbol{\sigma},u)-6(w+w_b)\tilde{P}(\boldsymbol{n},u). \tag{A3}$$

Assuming that

$$P(\boldsymbol{n}+\boldsymbol{\sigma},t=0)=\delta_{\boldsymbol{n},\mathbf{0}}\delta_{\boldsymbol{\sigma},\mathbf{0}}$$

and eliminating $\tilde{P}(\boldsymbol{n}+\boldsymbol{\sigma},u)$ from equations (A2) and (A3), we find

$$u\tilde{P}(\boldsymbol{n},u)-\delta_{\boldsymbol{n},\mathbf{0}}=\sum_{\boldsymbol{n}'}w\tilde{P}(\boldsymbol{n}',u)+\left(\frac{6w_b^2}{u+w_b}-6w-6w_b\right)\tilde{P}(\boldsymbol{n},u). \tag{A4}$$

Equation (A4) can be solved by introducing the Fourier transform, which leads to the solution (9).

References

[1] Mezei F, Knaak W and Farago B 1987 *Europhys. Lett.* **58** 571

[2] Kanaya T, Kawaguchi T and Kaji K 1992 *Physica* B **182** 403
Kanaya T, Kawaguchi T and Kaji K 1993 *J. Chem. Phys.* **98** 8262

[3] Tao N J, Li G and Farago B 1991 *Phys. Rev. Lett.* **66** 1334
Cummins H Z, Du W M, Fuchs F, Götze W, Hildebrand S, Latz A, Li G and Tao M J 1993 *Phys. Rev.* E **47** 4223
Kojima S, Yamaura T and Takagi Y 1997 *Proc. Yukawa Int. Seminar on Dynamics of the Glass Transition and Related Topics (1996); Prog. Theor. Phys. Suppl.* **126** 427

[4] Lunkenhiemer P, Pimenov A, Dressel M, Goncharov Yu G, Böhmer R and Loidl A 1996 *Phys. Rev. Lett.* **77** 318
Lunkenhiemer P, Pimenov A, Dressel M, Goncharov Yu G, Böhmer R and Loidl A 1997 *Proc. Yukawa Int. Seminar on Dynamics of the Glass Transition and Related Topics (1996); Prog. Theor. Phys. Suppl.* **126** 123

[5] Fujara F and Petry W 1987 *Europhys. Lett.* **4** 921
Buchenau U, Galperin Yu M, Gurevich V L, Parshin D A, Ramos M A and Schober H R 1992 *Phys. Rev.* B **46** 2798
Gil L, Ramos M, Bringer A and Buchenau U 1993 *Phys. Rev. Lett.* **70** 182

[6] Fujisaki M, Matsui J and Odagaki T 1997 *Proc. Yukawa Int. Seminar on Dynamics of the Glass Transition and Related Topics (1996); Prog. Theor. Phys. Suppl.* **126** 317

[7] Cole K S and Cole R H 1941 *J. Chem. Phys.* **9** 341

[8] Alder B J and Wainwright T E 1957 *J. Chem. Phys.* **27** 1208
Alder B J, Hoover H G and Young D A 1968 *J. Chem. Phys.* **49** 3988

[9] Higuchi M and Odagaki T 1997 *Proc. Yukawa Int. Seminar on Dynamics of the Glass Transition and Related Topics (1996); Prog. Theor. Phys. Suppl.* **126** 313
Higuchi M and Odagaki T 1997 *J. Phys. Soc. Japan.* **66** 3134

[10] Hiwatari Y, Miyagawa H and Odagaki T 1991 *Solid State Ion.* **47** 179

[11] Matsui J, Odagaki T and Hiwatari Y 1994 *Phys. Rev. Lett.* **73** 2452

[12] Matsui J, Fujisaki M and Odagaki T 1998 *Proc. 3rd Int. Discussion Mtg on Relaxation in Complex Systems; J. Non-Cryst. Solids* at press

[13] Odagaki T 1998 private communication

[14] Odagaki T, Matsui J and Hiwatari Y 1995 *Mater. Res. Soc. Symp. Proc.* **367** 337

[15] Odagaki T 1995 *Phys. Rev. Lett.* **75** 2452
Odagaki T 1997 *Proc. Yukawa Int. Seminar on Dynamics of the Glass Transition and Related Topics (1996); Prog. Theor. Phys. Suppl.* **126** 9

[16] Odagaki T and Hiwatari H 1991 *Phys. Rev.* A **41** 929